Analysis of various competing binary and ternary decay processes of the ^{253}Es nucleus

Nitin Sharma,* Amandeep Kaur, and Manoj K. Sharma
School of Physics and Materials Science, Thapar Institute of Engineering and Technology, Patiala 147004, Punjab, India

(Received 29 July 2020; accepted 28 September 2020; published 3 December 2020)

The ground state binary and ternary decays of the ^{253}Es radioactive nucleus are investigated using the quantum mechanical fragmentation theory (QMFT) based cluster decay models. First, the relative fragmentation of ^{253}Es is analyzed within the framework of the preformed cluster model (PCM). The PCM-calculated binary fragmentation structure is explored for two types of nuclear potential, i.e., Yukawa plus exponential and proximity potentials. The structure of the fragmentation potential and the location of potential minima are found to be independent of the choice of nuclear potential. It is observed from binary fragmentation structures that α (^{4}He) decay, cluster (^{46}Ar) emission, heavy particle (^{82}Ge) radioactivity, and spontaneous fission fragmentation (^{125}In) are the possible ground state decay modes of the ^{253}Es nucleus. The competitive emergence of these decay channels is explored by studying the preformation probability P_0, penetrability P, and half-lives $T_{1/2}$. The calculated half-lives of α and spontaneous fission match nicely with the experimental measurements. Also, the half-lives are predicted for cluster and heavy particle radioactivity, for which experimental verification would be of further interest. Further, an effort is made to explore the possibility of ternary fission (particle accompanied fission) for the decay of the ^{253}Es nucleus using the three-cluster model (TCM), where ^{4}He is observed to be the third fragment along with two binary fission fragments. A comparison of relative yields of binary and ternary fission confirm that the probability of the binary fission decay mode is larger than that of ternary fission. Moreover, closed shell effects play a significant role in the symmetric and asymmetric fission of binary and ternary fission, respectively.

DOI: 10.1103/PhysRevC.102.064603

I. INTRODUCTION

After the discovery of radioactivity by Becquerel [1] numerous radioactive nuclei were detected, and vast understanding of different kinds of radioactive decay was developed. It has been observed that the nuclei of the actinide region are radioactive, and exhibit α-decay, cluster emission, heavy particle radioactivity (HPR), and spontaneous fission (SF) [2–7]. The dominance of one or more such decay modes relies on the binding energy of parent nuclei and the fragmentation structure associated with them. After the establishment of α-decay and spontaneous fission processes, which are the traditional decay modes of unstable nuclei, the cluster decay mode, also called as cluster radioactivity (CR), came to be known in 1980 [4,5]. In this process, the radioactive nucleus decays via a fragment heavier than an α particle but smaller than the lightest fission fragment. Recently, another decay mode was predicted in which the size of the decaying fragment is heavier than a CR fragment and lighter than a fission fragment; it is known as heavy particle radioactivity (HPR) [6,7].

In general, the unstable nucleus splits into two binary fragments of comparable masses during the spontaneous fission process. Sometimes one finds three fragments in the outgoing channel instead of usual binary decay, and this process is known as ternary fission. Alvarez *et al.* discovered ternary fission for the first time in 1947 [8]. Generally, the studies suggest that the mass of the third fragment is much smaller than the other two main fission fragments, hence it is also known as light-particle-accompanied fission. In the most of the cases, the third fission fragment is usually an α particle due to its higher stability. To date, several theoretical and experimental investigations have been done to analyze the ternary fission of heavy and superheavy nuclei [9–12]. However, the mass yields with the most preferred fission fragments, which provide the structural information associated with the decaying fragments, are not studied extensively. Therefore, it would be interesting to analyze the dynamics of ternary breakup of a radioactive nucleus along with its usual binary fragmentation.

This paper aims to focus on the investigation of decay dynamics of the ^{253}Es radioactive nucleus [13]. To date, 17 isotopes of the einsteinium nucleus have discovered, i.e., $A = 241$–257, from a probable list of about a hundred isotopes [14]. The main properties of the ^{253}Es nucleus that we are interested in the present paper are fragment mass distribution and the half-lives of α decay, cluster radioactivity, heavy particle radioactivity, binary spontaneous fission, and ternary fission processes. In the present work, these binary decay mechanisms are analyzed within the framework of the preformed cluster model (PCM) [2,15]. The ^{253}Es nucleus is of interest because some relevant data on α decay and spontaneous fission processes are available. It is relevant to note that the half-lives of SF of the ^{253}Es nucleus are very

*nitinsharma2295@gmail.com

large as compared to the those for α decay. Hence, it has been difficult to obtain sufficiently strong sources for study because of the extremely high α-decay rates. The dynamic calculations incorporating both the fragmentation potential (or preformation probability) of the decaying nucleus and penetration probability of fragments are expected to impart useful insight for better understanding of the aforementioned phenomena. Moreover, it is clear from the literature that there are no thorough studies on the particle-accompanied ternary fission of einsteinium isotopes. Hence, the primary goals of present work are (i) to explore the binary fragmentation potential and preformation probability distribution for the competing analysis of α-decay, CR, HPR, and SF processes; (ii) to identify the decaying fragments and calculate their half-lives for all considered binary decay processes and compare with the experimental and other theoretical observations; (iii) to study the particle-accompanied ternary fission of the ^{253}Es isotope within the three-cluster model (TCM) [16,17], where the third fragment is fixed with mass $A = 4$; and (iv) to investigate the relative yields of both binary and ternary fission.

The overview of this paper is as follows. Section II describes the methodology used in this work. The collective clusterization approach of the preformed cluster model and the three-cluster model are briefly discussed, to analyze the binary and ternary decay mechanisms, respectively. The calculations and results of binary and ternary fragmentation are discussed in Sec. III. Finally, a summary of the observations and conclusions drawn are outlined in Sec. IV.

II. METHODOLOGY

The binary and ternary decay analyses of the ^{253}Es radioactive nucleus have been carried out within the preformed cluster model (PCM) [2,15] and the three-cluster model (TCM) [16,17], respectively. Both PCM and TCM approaches are based on the quantum mechanical fragmentation theory (QMFT) [18–20]. This theory considers the mass (and charge) asymmetry coordinate

$$\eta_A = \frac{A_1 - A_2}{A_1 + A_2} \quad \left(\text{and } \eta_Z = \frac{Z_1 - Z_2}{Z_1 + Z_2}\right) \tag{1}$$

as a dynamical coordinate for the mass and charge flow in the nuclear decay process. Subscripts 1 and 2 represent the heavy and light fragments. Another collective coordinate of this theory is relative separation (R) between the decay fragments. Note that these decay modes are based on collective clusterization criteria which treat all the decay mechanisms (e.g., light particles, intermediate mass fragments and fission fragments) on parallel footing. This aspect of handling various decay processes on parallel footing is not available in the majority of competing models.

A. Preformed cluster model (PCM)

The binary decay processes of ^{253}Es, such as α decay, cluster emission, binary spontaneous fission, etc., are studied within the PCM method. Based on the aforementioned coordinates, i.e., η and R, the collective fragmentation potential is calculated within the Strutinsky macroscopic-microscopic method [21] at fixed distance R_a (the first turning point of the penetration path), and given as

$$V_R(\eta) = \sum_{i=1}^{2} B(A_i, Z_i) + V_C\left(= \frac{Z_1 Z_2 e^2}{R}\right) + V_N. \tag{2}$$

$B(A_i, Z_i)$, the binding energies of two fragments, are the sum of the macroscopic liquid drop term (V_{LDM}) and the microscopic shell correction term (δU), and taken from the experimental compilation of Audi and Wapstra [22] and from the theoretical estimates of Möller *et al.* [23] whenever not available in [22]. In Eq. (2), the second term denotes the Coulomb potential and V_N is the nuclear attractive potential, explained further in Sec. II C.

The decay half-life $T_{1/2}$ and decay constant λ are obtained from following relation:

$$T_{1/2} = \frac{\ln 2}{\lambda} = \nu P_0 P. \tag{3}$$

Here, ν and P are the barrier assault frequency and barrier penetrability, respectively, where P refers to R motion. The preformation probability $[P_0 = |\psi(\eta(A_i))|^2 \sqrt{B_{\eta\eta}} \frac{2}{A_{CN}}]$ refers to η motion, which describes the probability of finding certain mass fragments at position R on the decay path. The P_0 is estimated by solving the Schrödinger equation in η coordinate using fragmentation potential as an input, at fixed $R = R_a$:

$$\left\{-\frac{\hbar^2}{2\sqrt{B_{\eta\eta}}}\frac{\partial}{\partial\eta}\frac{1}{\sqrt{B_{\eta\eta}}}\frac{\partial}{\partial\eta} + V_R(\eta)\right\}\psi^{\nu}(\eta) = E^{\nu}\psi^{\nu}(\eta), \tag{4}$$

with $\nu = 0, 1, 2, 3, \ldots$ referring to ground state ($\nu = 0$) and excited state ($\nu \neq 0$) solutions.

The penetration probability P of decaying fragments is obtained from Wenzel-Kramers-Brillouin (WKB) integral, and determined by following expression:

$$P = P_a W_i P_b, \tag{5}$$

Here, the transmission probability consists of three contributions as shown in Fig. 1:

(i) the penetrability P_a from R_a to R_i:

$$P_a = \exp\left[-\frac{2}{\hbar}\int_{R_a}^{R_i}\{2\mu[V(R) - V(R_i)]\}^{1/2}dR\right]; \tag{6}$$

(ii) the inner deexcitation probability W_i at R_i:

$$W_i = \exp(-bE_i); \tag{7}$$

(iii) and the penetrability P_b from R_i to R_b:

$$P_b = \exp\left[-\frac{2}{\hbar}\int_{R_i}^{R_b}\{2\mu[V(R) - Q]\}^{1/2}dR\right]. \tag{8}$$

This indicates that the penetration process begins at $R = R_a$ and terminates at $R = R_b$ with $V(R_b) = Q$ value. The concept of de-excitation probability W_i is taken from the excitation model of Griener *et al.* [24]. In Eq. (7), E_i is the excitation energy of the daughter nucleus, which is the energy difference between $V(R_i)$ and the Q value of the decay products. At this point, the excitation of the daughter nucleus is a consequence of nuclear and Coulomb interactions of the decaying fragments. Furthermore, if parameter b of Eq. (7) was allowed

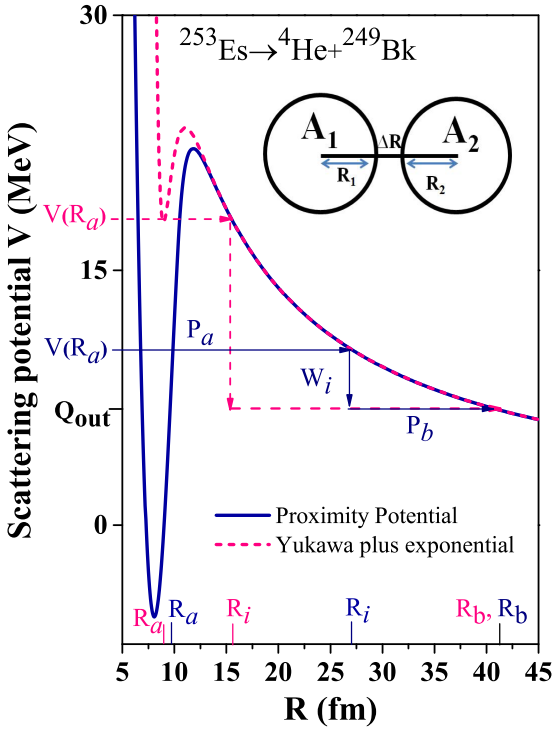

FIG. 1. The binary scattering potential $V(R)$ for the α decay of the ^{253}Es nucleus for two kinds of nuclear potential, i.e., Yukawa plus exponential and proximity potentials. Also, the schematic representation of all the parameters is given.

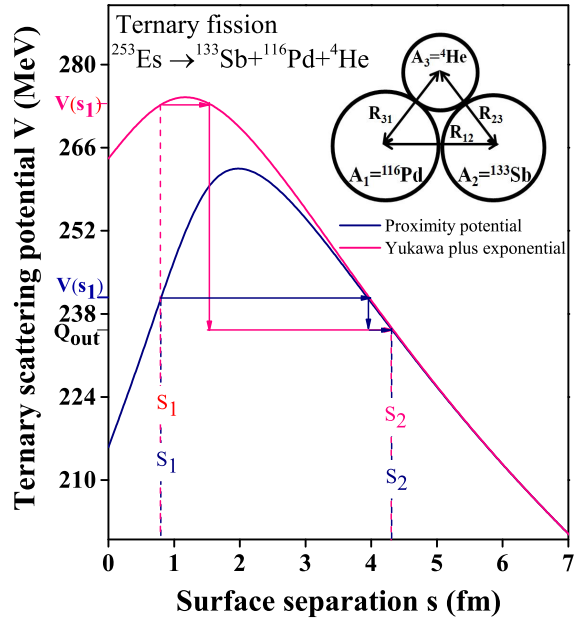

FIG. 2. The ternary fission scattering potential V (MeV) as a function of surface separation (s) for ^{253}Es is plotted with the use of Yukawa plus exponential and proximity nuclear potentials.

to depend on R_i (see Fig. 2 of Ref. [24]), then it should become a process of multiple de-excitations and proceed as a steplike process. In the present work, the de-excitation of the daughter nucleus is restricted to only a single transition. The parameter b is taken to be negligibly small which means that the excitation of the decay fragments plays a minor role, and hence $W_i = 1$. The first turning point R_a is defined as $R_a = R_1 + R_2 + \Delta R$. Here R_1 and R_2 are the radii of decaying fragments and are calculated as $R_i = 1.16A_i^{1/3}$. ΔR is the relative separation distance between two fragments or clusters and is supposed to assimilate the neck formation effects, and hence is referred to as the neck-length parameter.

B. Three-cluster model (TCM)

Recently, the TCM was developed by Manimaran *et al.* [16,17], as an extension of the preformed cluster model. It also works out in terms of mass (η_A) and charge (η_Z) asymmetry coordinates. For the case of ternary fission, the third fragment which is represented by A_3 is fixed, and hence mass and charge asymmetry is considered only between A_1 and A_2. The relative separation among the three fragments is $R_{ij}^s = R_{ij} + s_{ij}$ where $R_{ij} = r_0(A_i^{1/3} + A_j^{1/3})$ ($r_0 = 1.16$ fm) and s_{ij} is the surface separation between decaying fragments. s_{ij} is considered to be zero for the touching equatorial configuration of three fragments, as shown in Fig. 2. The fragmentation potential for the equatorial configuration of ternary fission decay is calculated as

$$V_{tot} = \sum_{i=1}^{3}\sum_{j>i}^{3} B_i + V_{Cij}\left(= \frac{Z_i Z_j e^2}{R_{ij}}\right) + V_{Nij}. \tag{9}$$

The penetration probability of the ternary fragments crossing the potential barrier is estimated as [17]

$$P = \exp\left[-\frac{2}{\hbar}\int_{s_1}^{s_2}\{2\mu_{123}[V(s) - Q]\}^{1/2} ds\right]. \tag{10}$$

s_1 is a first turning point and s_2 is the second turning point satisfying $V(s_2) = Q$ as shown in Fig. 2. The Q value for the decay of three fragments is obtained as $Q = M - \sum_{i=1}^{3} m_i$. In Eq. (10), μ_{123} is the reduced mass of three fragments,

$$\mu_{123} = \left(\frac{\mu_{12}A_3}{\mu_{12} + A_3}\right)m, \tag{11}$$

where $\mu_{12} = A_1A_2/(A_1 + A_2)$ and m is the nucleon mass.

The relative yields for all the fragmentation channels for both binary and ternary decay processes are calculated as the ratio between the penetration probability of a given fragment over the sum of penetration probabilities of all possible fragmentations as [17]

$$Y(A_i, Z_i) = \frac{P(A_i, Z_i)}{\Sigma P(A_i, Z_i)}. \tag{12}$$

C. Nuclear potential

In Eqs. (2) and (9), V_{Nij} is the attractive nuclear potential. In the present work, two different types of attractive nuclear potentials are used for the calculations. The first is the short-range Yukawa plus exponential nuclear potential, which is

given as [25]

$$V_{Yij} = -4\left(\frac{a}{r_0}\right)^2 \sqrt{a_{2i}a_{2j}}[g_i g_j(4+\xi) - g_j f_i - g_i f_j] \times \frac{\exp(-\xi)}{\xi}, \quad (13)$$

where $\xi = R^s_{ij}/a$, and the functions g and f are

$$g_k = \zeta \cosh\zeta - \sinh\zeta \quad (14)$$

and

$$f_k = \zeta^2 \sinh\zeta, \quad (15)$$

where $\zeta = R_k/a$ with the radius of the nucleus being $R_k = r_0 A_k^{1/3}$. Here $a = 0.68$ is the diffusivity parameter and the asymmetry parameter is $a_{2k} = a_s(1 - \omega I^2)$ with $a_s = 21.13$ MeV, $\omega = 2.3$, and $I = \frac{N-Z}{A}$.

Alternatively we have used the nuclear proximity potential from Ref. [26]. It reads as

$$V_{Pij}(s) = 4\pi \overline{R}\gamma b\Phi(s), \quad (16)$$

where s is the surface separation of fragments, $\gamma = 0.9517[1 - 1.7826(N - Z/A)^2]$ MeV fm^{-2} is the surface energy constant, and $b = 0.99$ is the nuclear surface thickness. $\overline{R}$ is the mean curvature radius and Φ is the universal function; for more details, see Ref. [27]. The fragmentation potential using these nuclear potentials is calculated for both binary and ternary decays, and the relevant results are discussed in Sec. III.

III. CALCULATIONS AND DISCUSSIONS

This section represents the theoretical investigation of binary and ternary decay mechanisms of the ^{253}Es nucleus within the cluster-decay models. First, in Sec. III A, the competing analysis is carried out for various decay modes of ^{253}Es such as α decay, cluster radioactivity (CR), heavy particle radioactivity (HPR), and spontaneous fission (SF). The fragmentation structure is analyzed to explore all the possible fragment emissions. The decaying fragments are identified and their corresponding half-lives are calculated and compared with available experimental and other theoretical observations. It is worth mentioning here that such fragment identification is not available in the reported experiments for cluster, HPR, and SF cases; also no experimental information is available for the half-lives of CR and HPR channels. The calculations are made using two kind of nuclear potentials, i.e., Yukawa plus exponential and proximity potentials within the framework of PCM. Further, Sec. III B presents the calculations for the particle-accompanied ternary fission of ^{253}Es for the equatorial configuration using TCM (see Fig. 2). Also, the relative yield is calculated, and decaying fission fragments are identified in terms of mass and charge numbers. Finally, a comparative analysis of binary and ternary fission is made in Sec. III C.

A. Competing binary decay mechanisms of ^{253}Es nucleus

First, the barrier characteristics for the α decay of the ^{253}Es nucleus are analyzed by plotting the scattering potential in Fig. 1 for both Yukawa plus exponential and proximity nuclear potentials. It is evident that the two potentials show different barrier characteristics. The barrier position and barrier height are different for the two cases, and hence the penetrability probability gets modified accordingly. The Coulomb barrier is smaller for the case of the proximity potential, and one can say that the probability of α emission is higher for that case. A similar trend can be seen from Fig. 2 for the case of ternary fission of the ^{253}Es nucleus.

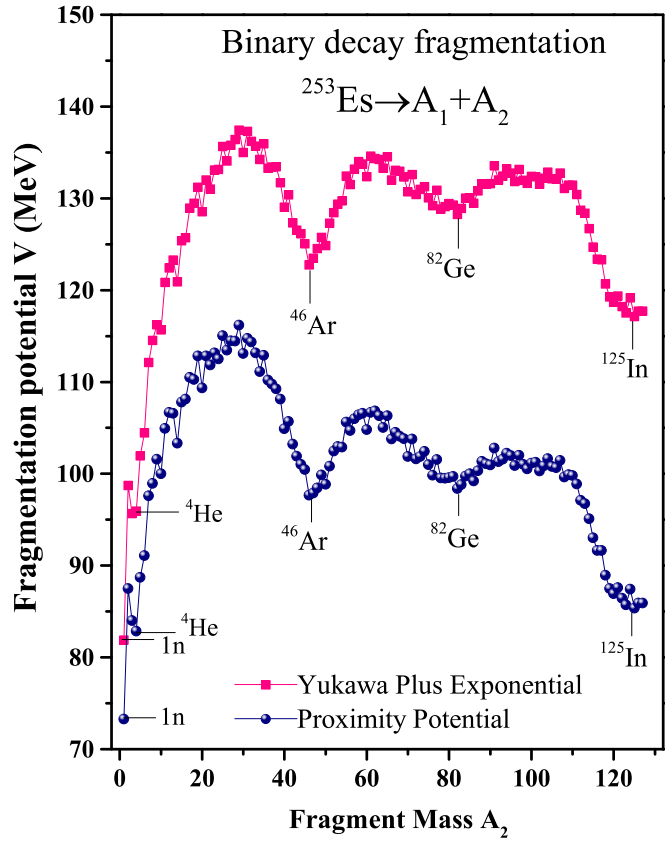

FIG. 3. Binary fragmentation potential V (MeV) as a function of fragment mass A_2 for ^{253}Es nucleus calculated using Yukawa plus exponential and proximity potentials. The deepest minima of the fragmentation potential are also marked.

The collective illustration of a nuclear dynamics is exploited by studying the fragmentation potential and preformation probability. In order to examine the dynamics of the radioactive nucleus, the collective potential energy (or fragmentation potential) is calculated, which is the key ingredient to the Schrödinger equation [see Eq. (4)]. By studying the deep valleys in the fragmentation potential at all η values, the relative stability of decaying fragments can be estimated. Thereby, the binary fragmentation potential $V_R(\eta)$ (MeV) of ^{253}Es was calculated, and the results are plotted in Fig. 3. The investigation of fragmentation potential is carried out for both Yukawa plus exponential and proximity nuclear potentials. A deep analysis of the prominent dips in the fragmentation plot leads to the observation that most preferred decay fragments are the same for both choices of nuclear potential. However, there is a significant difference in the magnitude of

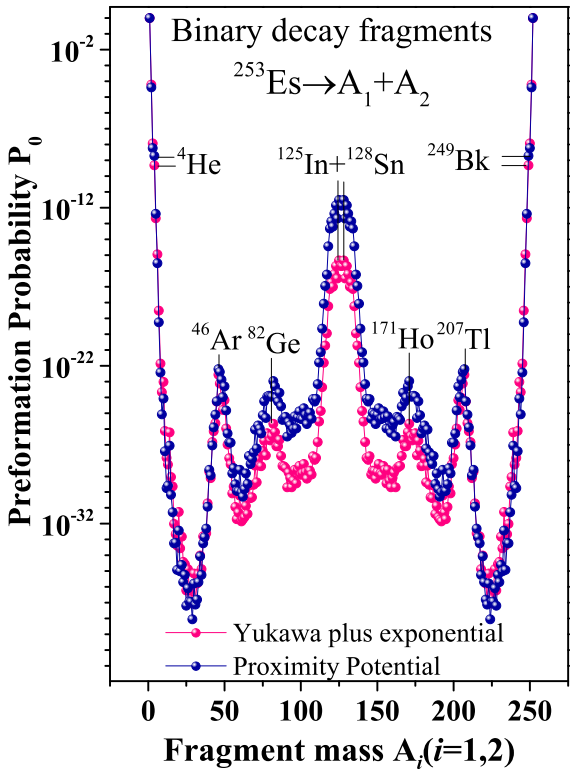

FIG. 4. Preformation probability P_0 as a function of fragment mass A_i for the ^{253}Es nucleus calculated using Yukawa plus exponential and proximity potentials.

fragmentation potential. It is evident from Fig. 3 that the clusters or fragments corresponding to the deepest minima of the fragmentation potential are $1n$, ^{4}He, ^{46}Ar, ^{82}Ge, and ^{125}In. The α particle (^{4}He) along with the $1n$ have lower fragmentation potential. However, the present work aims primarily to explore the relative abundance of radioactive processes, so only α decay is compared to heavier cluster emissions. As stated above, the decay fragments for CR, HPR, and SF decays are identified, respectively, as ^{46}Ar, ^{82}Ge, and ^{125}In (along with complementary fragments).

Figure 4 represents the PCM-calculated preformation probability P_0 as a function of fragment mass A_i for binary decays of ^{253}Es using Yukawa plus exponential and proximity potentials. The minima in the fragmentation potential correspond to the maxima in the profile of preformation probability P_0. This indicates that the fragment having the highest value of preformation probability forms the most favorable fragment in the exit channel. The decaying fragments are identified as marked in the preformation plot. The spontaneous fission decay of the ^{253}Es nucleus favors symmetric fragmentation (^{125}In + ^{128}Sn channel), and this choice of most probable fission fragments depicts the importance of closed shell effects near $Z = 50$. The reason behind the emergence of the predicted clusters and/or fragments is apparently due to the magicity of the corresponding daughter products in all the decay channels.

The competing nature of all four decay channels of ^{253}Es can be seen from Figs. 5(a)–(c), which show the behavior of fragmentation potential, preformation probability P_0, and barrier penetrability P (calculated at the corresponding fitted ΔR's). It is observed from Fig. 5(a)that the α and spontaneous fission fragment (^{125}In) have lower magnitude of fragmentation potential than the cluster (^{46}Ar) and heavy fragment (^{82}Ge). Consequently, the magnitude of P_0 is larger for the α and SF fragment than other two decay channels, which means the probability of α emission and SF decay channels is higher for the ^{253}Es nucleus. However, Fig. 5(c) depicts that barrier penetrability increases with increase in mass number of decay fragment. It is noticed that proximity and Yukawa nuclear potentials show similar structural behavior for all kinds of binary decay processes (also shown in Fig. 3). However, there is a significant difference in magnitude. Knowing that half-lives are the combined effect of preformation probability P_0 and penetrability P, the PCM-calculated results are presented in Table I. The half-lives of the α and fission fragment are smaller than those of the cluster and heavy fragment, as shown

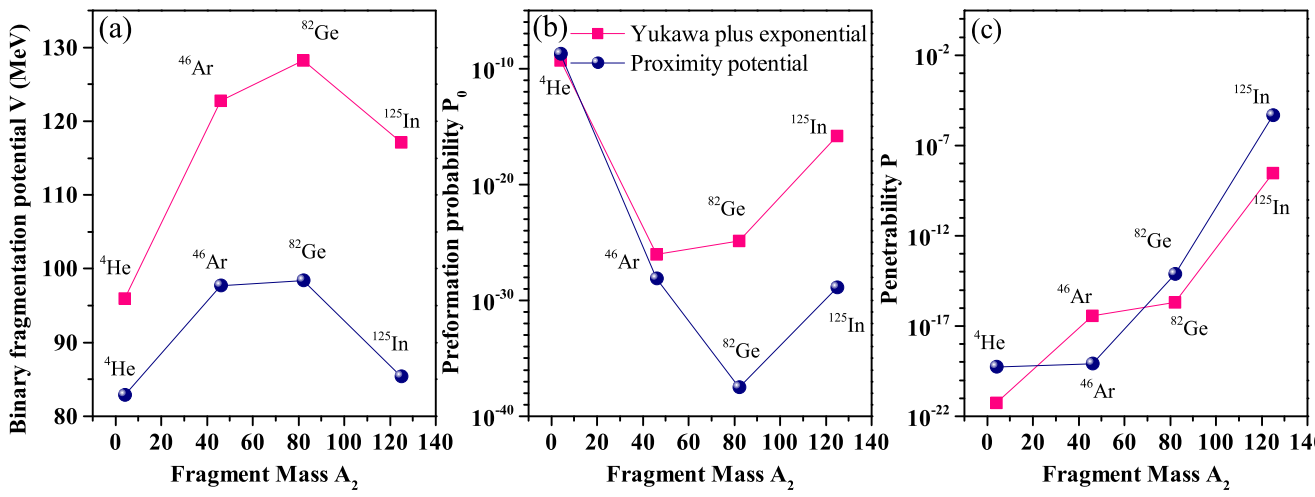

FIG. 5. The competitive analysis of all the binary decay mechanisms (α, CR, HPR, and SF) via (a) binary fragmentation potential V (MeV), (b) preformation probability P_0, and (c) penetrability P as a function of fragment mass A_2.

TABLE I. PCM-calculated half-lives of α, CR, HPR, and SF decay channels of the ^{253}Es nucleus are compared with the experimental data [28,29] and other theoretical observations [30]. The optimized values of neck-length parameter ΔR with other calculated quantities are also presented in the table.

Decay mode	Decay channel	Q value (MeV)	ΔR (fm)		Half-lives $\log_{10} T_{1/2}$ (s)			
			Yukawa	Proximity	Yukawa (PCM)	Proximity (PCM)	Expt.	Theoretical
α	^{4}He + ^{249}Bk	6.75	−0.20	0.75	9.0	6.45	6.2	7.16 [30]
Cluster	^{46}Ar + ^{207}Tl	128.7	0.70	−0.85	20.81	25.54		24.37 [30]
HPR	^{82}Ge + ^{171}Ho	199.2	−0.40	−1.0	19.94	30.03		
SF	^{125}In + ^{128}Sn	243.3	−0.40	−1.0	2.77	12.65	13.29	

in the table. However, the half-lives for the α and SF channels show nice agreement with the experiment measurements [28,29] with the use of the proximity potential. This is due to the different barrier characteristics of the two the potentials, as shown in Fig. 1. The best-fitted values of neck-length parameter and Q value for all the binary decay channels are presented in Table I. The comparison of PCM-calculated half-lives with other theoretical observations [30] is also made.

B. Decay of ^{253}Es through ternary fragmentation

In this section, the possibility of ternary decay of the ^{253}Es nucleus is investigated, within the three-cluster model (TCM) [16,17]. The ternary fragmentation potential using Eq. (9) is calculated for the considered radioactive nucleus using the assumption of equatorial configuration [16], and plotted in Fig. 6 as a function of fragment mass A_2. The calculations are made at surface separation $s = 0.8$ fm as the scattering potential

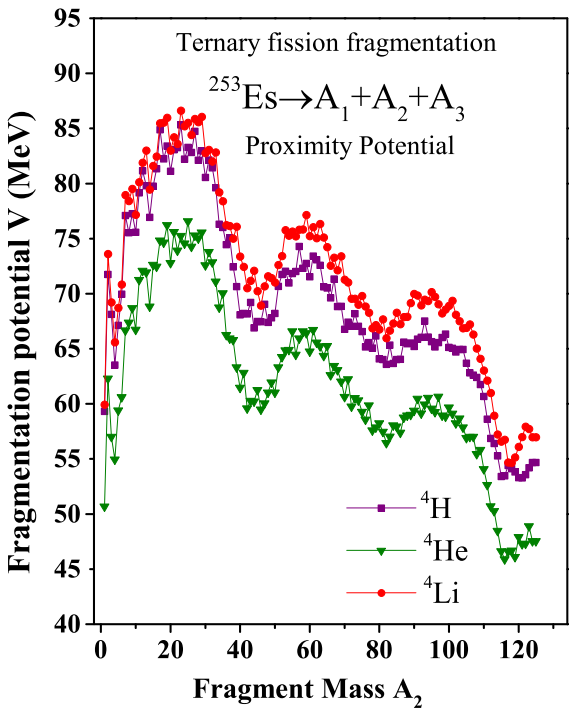

FIG. 6. Ternary fragmentation potential V (MeV) as a function of fragment mass for ^{253}Es for different $A_3 = 4$ combinations.

$V(s_1)$ corresponding to first turning point s_1 should be greater than the Q value of the decay process for the penetration of the barrier to occur. Note that the third fragment mass is fixed, i.e., $A_3 = 4$, and the possible choices of fragments for mass number 4 are taken as ^{4}H, ^{4}He, and ^{4}Li. As mentioned in Sec. II B, the fragmentation potential is minimized in mass-charge asymmetry coordinates for the remaining two binary fragments ($A_1 + A_2$). It is evident from the figure that the magnitude of ternary fragmentation potential is lower for $A_3 = {}^{4}$He (than ^{4}H and ^{4}Li fragments). This indicates that the $A_3 = {}^{4}$He accompanied ternary fission is most favored for the ^{253}Es nucleus. This preference of the ^{4}He fragment as a third fragment for the ternary decay of the considered nucleus is in accordance with [31]. Hence, the further investigation is carried out by considering ^{4}He as a third fragment for the ternary fission decay of the ^{253}Es nucleus.

Next, to analyze the ternary decay of ^{253}Es, we have considered two nuclear potentials, i.e., Yukawa plus exponential and proximity potentials, as discussed in Sec. II C. In Fig. 7, the ternary fragmentation potential is plotted as a function of fragment mass A_2 for both types of nuclear potential. Note that results shown in Fig. 7 are calculated at common surface separation $s = 0.8$ fm. It is clearly evident from the figure that the magnitude of the fragmentation potential is small for the attractive proximity potential as compared to the Yukawa plus exponential potential. That means the probability of ternary emission seems higher for the choice of the proximity potential. However, the fragmentation structure and the choice of most probable $A_1 + A_2$ fragments are the same for both cases, where the third fragment is fixed ($A_3 = {}^{4}$He). The minima of the fragmentation path (say, using the proximity nuclear potential) of the ^{253}Es nucleus correspond to the following combinations ($^{253}\text{Es} \rightarrow A_1 + A_2 + A_3$):

(i) $^{253}\text{Es} \rightarrow {}^{4}\text{He}(Z{=}2, N{=}2) + {}^{46}\text{Ar}(Z{=}18, N{=}28) + {}^{203}\text{Au}(Z{=}79, N{=}124)$,

(ii) $^{253}\text{Es} \rightarrow {}^{4}\text{He}(Z{=}2, N{=}2) + {}^{82}\text{Ge}(Z{=}32, N{=}50) + {}^{167}\text{Tb}(Z{=}65, N{=}102)$,

(iii) $^{253}\text{Es} \rightarrow {}^{4}\text{He}(Z{=}2, N{=}2) + {}^{116}\text{Pd}(Z{=}46, N{=}70) + {}^{133}\text{Sb}(Z{=}51, N{=}82)$.

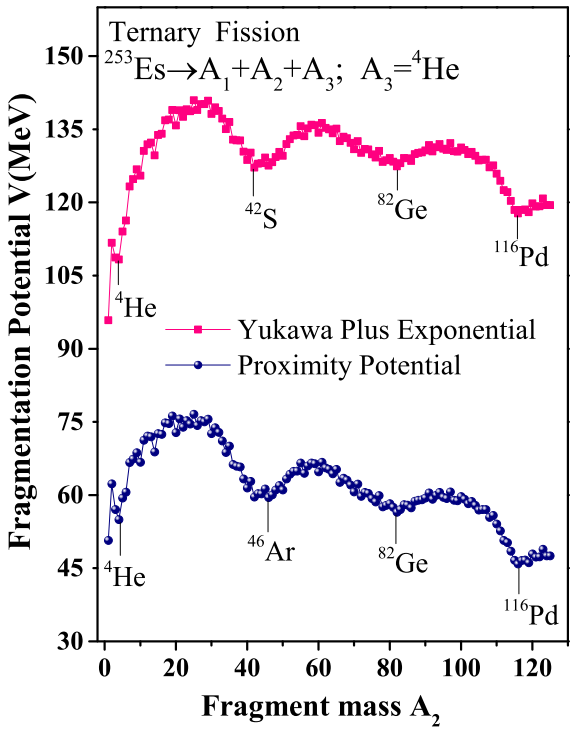

FIG. 7. Ternary fragmentation potential $V(A_2)$ of ^{253}Es for Yukawa plus exponential and proximity nuclear potentials.

In cases (i), (ii), and (iii), the emergence of minima is associated with neutron magicity $N = 28$, 50, and 82 respectively. Here, ^{4}He (doubly magic nucleus) is considered as the third fragment in ternary decay. These results indicate the conclusive role of closed-shell effects in the ternary fission fragmentation of ^{253}Es. An experimental verification of these results would be of future interest.

C. Comparative analysis of binary and ternary fission

Finally, a comparative analysis of binary and ternary fission of the ^{253}Es nucleus is carried out in this section. The relative yields [as per Eq. (12)] of binary and ternary fission fragments are calculated and the results are shown respectively in Figs. 8(a) and 8(b). The scales of x and y axes are same in both panels so that one-to-one comparison of binary and ternary fission mechanisms can be carried out. As per Figs. 3 and 7, the binary and ternary fission decays are more prominent for the proximity potential, hence the calculations are done for this choice of potential. The fission fragment mass distribution is significantly different for binary and ternary fission. Ternary fission fragmentation is more asymmetric as compared to binary fission. The choice of most probable fragment, as marked in the figure, is also different for the considered fission decay mechanisms. Clearly, the relative yield of symmetric fragments is higher for the case of binary fission decay relative to ternary fission. This observation also suggests that the possibility of binary fission is higher as compared to ternary fission.

IV. SUMMARY

Summarizing, the preformed cluster model (PCM) and the three-cluster model (TCM) are used to study the binary and ternary decay processes of the ^{253}Es nucleus. The binary decay mechanisms (such as α, cluster, HPR, SF) are explored by calculating the fragmentation potential and preformation probability using PCM. The choice of most probable

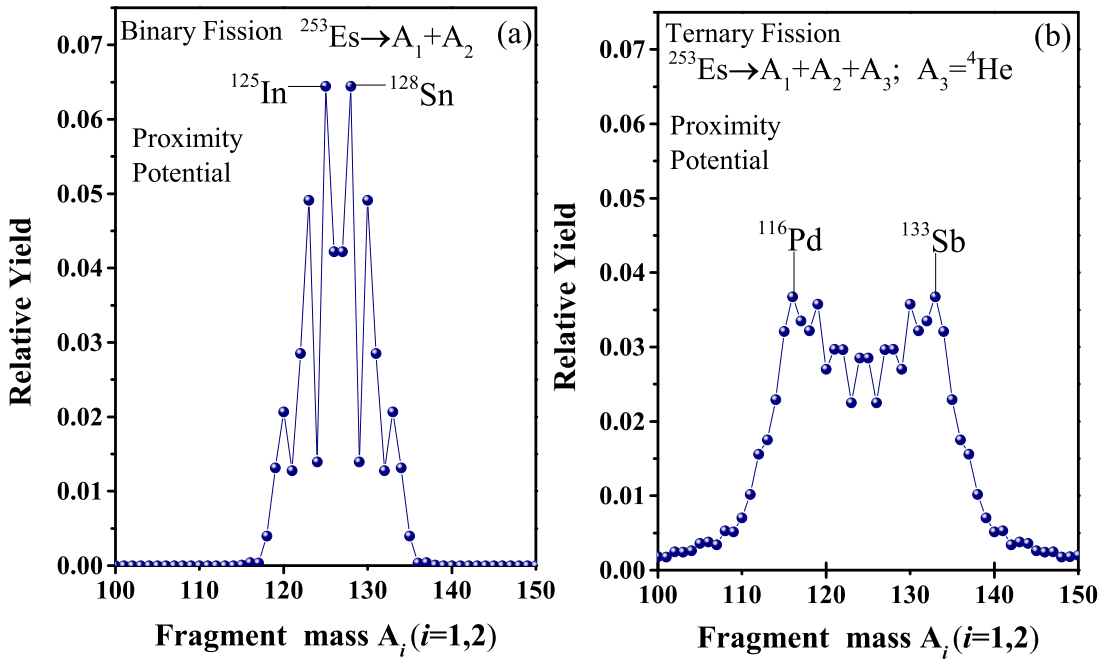

FIG. 8. The calculated relative yields for (a) binary fission and (b) ternary fission of ^{253}Es. The most probable fission fragments are also marked.

fission fragments depicts the importance of closed shell effects. The calculations are performed using two kinds of attractive nuclear potentials, i.e., Yukawa plus exponential and proximity potentials. It is observed that the two nuclear potentials have different barrier characteristics. As a result, the PCM-calculated half-lives of α and SF channels show nice agreement with experimental results using the proximity potential. However, the half-lives are predicted for cluster and heavy particle radioactivity. Apart from this, ternary fission is studied using TCM for the ^{253}Es nucleus. It is observed that ^{253}Es may also decay via particle-accompanied fission, where the third particle is identified as ^{4}He. Further, a comparative analysis of both binary and ternary fission is carried out. The relative yield of symmetric binary fragments is higher than in ternary fission. The most probable decay fragments are identified for binary as well as ternary cases. Finally, it is observed that magic shell effects near $Z = 50$ and $N = 82$ play an important role in the choice of binary as well as ternary fission. It will be of further interest to incorporate deformation effects in the binary and ternary decay analysis.

ACKNOWLEDGMENT

Financial support from the UGC-DAE Consortium for Scientific Research, File No. UGC-DAE-CSR-KC/CRS/19/NP09/0920, is gratefully acknowledged.

[1] A. Allisy, Radiat. Prot. Dosim. **68**, 3 (1996).
[2] K. Sharma, G. Sawhney, and M. K. Sharma, Phys. Rev. C **96**, 054307 (2017).
[3] A. Kaur, G. Sawhney, and M. K. Sharma, Int. J. Mod. Phys. E **27**, 1850043 (2018).
[4] A. Sandulescu, D. N. Poenaru, and W. Greiner, Sov. J. Part. Nucl. Phys. **11**, 528 (1980).
[5] H. J. Rose and G. A. Jones, Nature (London) **307**, 245 (1984).
[6] D. N. Poenaru, R. A. Gherghescu, and W. Greiner, Phys. Rev. Lett. **107**, 062503 (2011).
[7] D. N. Poenaru, R. A. Gherghescu, and W. Greiner, Phys. Rev. C **85**, 034615 (2012).
[8] L. W. Alvarez, as reported by G. Farewell, E. Segre, and C. Wiegand, Phys. Rev. **71**, 327 (1947).
[9] K. Manimaran and M. Blasubramaniam, J. Phys. G **37**, 045104 (2010).
[10] K. Manimaran and M. Blasubramaniam, Eur. Phys. J. A **45**, 293 (2010).
[11] A. V. Ramayya, J. K. Hwang, J. H. Hamilton, A. Sandulescu, A. Florescu, G. M. Ter-Akopian, A. V. Daniel, Y. T. Oganessian, G. S. Popeko, W. Greiner, and J. D. Cole, Phys. Rev. Lett. **81**, 947 (1998).
[12] Yu. N. Kopatch, M. Mutterer, D. Schwalm, P. Thirolf, and F. Gonnenwein, Phys. Rev. C **65**, 044614 (2002).
[13] S. G. Thompson, A. Ghiorso, B. G. Harvey, and G. R. Choppin, Phys. Rev. **93**, 908 (1954).
[14] D. Meierfrankenfeld, A. Burya, and M. Thoennessen, At. Data Nucl. Data Tables **97**, 134 (2011).
[15] G. Sawhney, K. Sandhu, M. K. Sharma, and Raj K. Gupta, Eur. Phys. J. A **50**, 175 (2014).
[16] K. Manimaran and M. Balasubramaniam, Phys. Rev. C **79**, 024610 (2009).
[17] K. Manimaran and M. Balasubramaniam, Phys. Rev. C **83**, 034609 (2011)
[18] J. Maruhn and W. Greiner, Phys. Rev. Lett. **32**, 548 (1974).
[19] R. K. Gupta, W. Scheid, and W. Greiner, Phys. Rev. Lett. **35**, 353 (1975).
[20] R. K. Gupta, A. Sandulescu, and W. Greiner, Phys. Lett. B **67**, 257 (1977)
[21] V. M. Strutinsky, Nucl. Phys. A **95**, 420 (1967).
[22] G. Audi and A. H. Wapstra, Nucl. Phys. A **595**, 409 (1995).
[23] P. Möller, J. R. Nix, W. D. Myers, and W. J. Swiatecki, At. Nucl. Data Tables **59**, 185 (1995).
[24] M. Greiner and W. Scheid, J. Phys. G **12**, L229 (1986).
[25] G. Shanmugam and B. Kamalharan, Phys. Rev. C **38**, 1377 (1988).
[26] J. Blocki, J. Randrup, W. J. Swiatecki, and C. F. Tsang, Annals of Physics **105**, 427 (1977).
[27] R. K. Gupta, N. Singh, and M. Manhas, Phys. Rev. C **70**, 034608 (2004).
[28] https://www.nndc.bnl.gov/.
[29] N. E. Holden and D. C. Hoffman, Pure Appl. Chem. **72**, 1525 (2000).
[30] G. M. Carmel, V. Bai, and R. N. Agnes, Pramana J. Phys. **88**, 43 (2017).
[31] T. R. England and B. F. Rider, Evaluation and Compilation of Fission Product Yields 1993, Los Alamos National Laboratory Report No. LA-SUB94-170 (unpublished).